Mon. Not. R. Astron. Soc. **382,** 553–566 (2007) doi:10.1111/j.1365-2966.2007.11852.x

The abundances of nearby red clump giants⋆

Y. J. Liu,[1,2] G. Zhao,[1]† J. R. Shi,[1] G. Pietrzyński[3,4] and W. Gieren[3]

[1]*National Astronomical Observatories, Chinese Academy of Sciences, Beijing 100012, China*
[2]*Graduate University of Chinese Academy of Sciences, Beijing 100049, China*
[3]*Departamento de Física, Universidad de Concepción, Casilla 160-C, Concepción, Chile*
[4]*Warsaw University Observatory, AL. Ujazdowkie 4, PL-00-478 Warsaw, Poland*

Accepted 2007 April 2. Received 2007 February 13; in original form 2006 September 13

ABSTRACT

Based on the analysis of high-resolution spectra with a high signal-to-noise ratio, we have determined the abundances of the α-elements O, Si, Ca and Ti, the iron peak elements V, Fe and Ni, and the heavy element Ba without the consideration of non-local thermodynamic equilibrium (NLTE) effect and the light neutron-rich elements Na, Mg and Al with an NLTE analysis for 63 nearby red clump giants. Fe abundances cover a logarithmic range between -0.60 and $+0.35$ relative to solar. All abundance ratios with respect to Fe are similar to those found in the Sun. Hyperfine structure (HFS) was taken into account when calculating V lines. The difference in abundances obtained with and without HFS can be as large as 0.5 dex.

Key words: stars: abundances – stars: atmospheres – stars: late-type.

1 INTRODUCTION

The chemical evolution of the Milky Way is dominated by nucleosynthesis yields often propagated through many generations of stars. Tinsley & Larson (1979) proposed a scenario of chemical evolution of galaxies, which predicted that iron group elements are ejected from long-lived Type Ia supernovae (SNe Ia, resulting from mass accretion by a C-O white dwarf). Their progenitor stars have longer lifetimes than those of SNe II (resulting from exploding massive stars). The nucleosynthesis theory predicts that SN II yields produce an [α/Fe] overabundance in metal-poor stars, and this has been proved as reasonable in observations (e.g. McWilliam 1997, and references therein).

Differences among abundance ratios in different stages of stellar evolution are of great significance in providing clues to the processes of nucloesynthesis and Galaxy evolution. Thus, studying stars in their post-main-sequence stage is very important for us to understand stellar structure and evolution, and determining elemental abundance patterns is essential to comprehend more about the chemical evolution of the Galaxy. Red clump giants belong to those low-mass stars that are experiencing core-helium burning after the red giant stage and the helium flash. Therefore, their surface abundances are the results of convective mixing and envelope ejection. Whether the element abundances, especially those of the α-elements, oxygen and sodium, are consistent with the theoretical predictions needs to be tested by high-resolution spectral analysis. There have been only a few papers analysing elemental abundances other than iron in red clump giants. This paper is focusing on the discussion of 10 elemental abundances in red clump giants obtained through the analysis of high-resolution and high signal-to-noise ratio (S/N) spectra.

2 OBSERVATION AND DATA REDUCTION

We selected 76 Southern hemisphere stars from Paczyński et al. (1999) who published a sample of 308 red clump giants selected from the *Hipparcos* catalogue with a relative parallax error of less than 10 per cent. The stars were observed with the Fiber-fed Extended Range Optical Spectrograph (FEROS), which was attached to the 1.52-m telescope of the ESO (La Silla, Chile), in 2002 August. FEROS has very high efficiency and a large wavelength coverage, from 3800 to 9000 Å, and it also has a sufficient resolving power of $R = 48\,000$. Unfortunately, the spectral quality in the blue part is not good enough, and we only used spectra with wavelengths longer than 5200 Å in this study except for Mg λλ4571, 4702. Most of our samples have S/N > 100. Fig. 1 shows the spectrum of HIP 86391 in the region of the oxygen triplet. We removed 13 stars, among which 11 are variable or multiple stars, and two have extremely bad spectra. Finally, 63 stars are left in our sample.

The ESO's MIDAS/ECHELLE software was used as our standard data-reduction package. A completely automatic online reduction is available, and we adopted it. After the automatic reduction, we get one-dimensional spectra, from which the radial velocity shift was measured using at least 20 pre-selected lines. The spectra were normalized with a continuum function determined by fitting a spline curve to a set of pre-selected continuum windows (typically 10–20 per order), which were taken from a typical late-type giant spectrum. There are two methods to measure the equivalent width (EW)

⋆Based on observations collected at the European Southern Observatory (ESO) 1.52-m telescope at the La Silla Observatory in 2002 August.
†E-mail: gzhao@bao.ac.cn

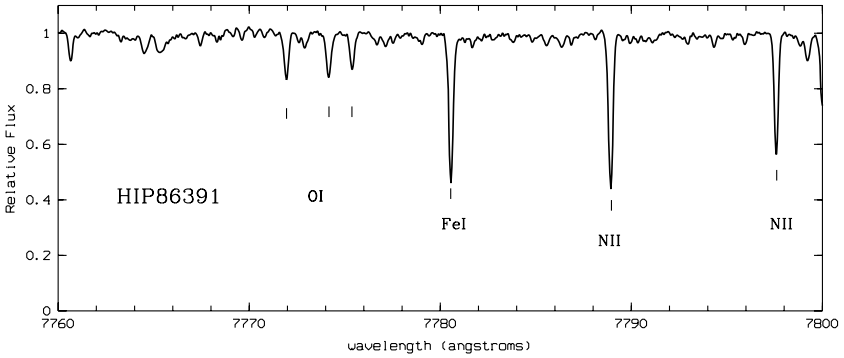

Figure 1. A portion of spectrum obtained with the FEROS for HIP 86391 ($T_{\rm eff} = 4829, \log g = 2.86$, [Fe/H] $= 0.14$ and $\xi_{\rm t} = 1.2$, S/N ~ 150).

of the spectral lines we used in this study: direct integration of the line profile and fitting by a Gaussian function. The direct integration method is suitable for strong unblended lines while the Gaussian function fit is appropriate for weak lines, <20 mÅ. The final values of the EWs were selected depending on which method gave the best fit to the line profile (see Table 1 in the electronic version of this paper on *Synergy* – see the Supplementary Material section).

The comparison of our EWs for HIP 3455 with those from Zhao, Qiu & Zhang (2001a) for 85 lines in common is displayed in Fig. 2. The systematic difference between the two sets of data is small and a linear least-squares fit gives $\mathrm{EW_{LIU}} = 1.034\ (\pm 0.015)\,\mathrm{EW_{ZHAO}} - 2.148\ (\pm 1.447)$, with the standard deviation of 4 mÅ.

3 STELLAR ATMOSPHERIC PARAMETERS

To establish the stellar atmospheric model, we need basic stellar parameters, namely, effective temperature, surface gravity, metallicity and microturbulence velocity.

3.1 Effective temperature

Effective temperatures were derived from the photometric colour index $B - V$ and [Fe/H] using the empirical calibration given by a corrected relation of Alonso, Arribas & Martínez-Roger (2001). Their work shows that the effective temperature resulting from $V - K$ is more accurate than other colour indices for giant stars. However, the measured error for the $K_{\rm s}$-band magnitudes taken from the Two-Micron All-Sky Survey (2MASS)[1] is higher than 0.2 mag for most of our samples, and a 0.2-mag error in the $K_{\rm s}$ band causes an error of about 250 K in effective temperature. The transformation between 2MASS ($K_{\rm s}$ magnitude, see detailed in Persson et al. 1998) and the CIT system (K magnitude) was provided by Carpenter (2001). Such a big measurement error in the $K_{\rm s}$ magnitude from 2MASS is due to the fact that the $K_{\rm s}$ magnitudes of most of our giants are brighter than 4 mag. For those stars, whose images saturated even on the 51-ms exposure, $K_{\rm s}$-band indices have much larger uncertainties because the fluxes were extracted with a procedure that fits to the scattered light wings of the saturated stellar profiles (Cutri et al. 2003; Skrutskie et al. 2006). On the other hand, as shown in Alonso, Arribas & Martínez-Roger (1999), effective temperatures determined from $b - y$ are more accurate than those from $B - V$. Unfortunately, only 21 stars with $b - y$ index are available in our sample. Therefore, using $B - V$ to determine the temperatures seemed to be the only choice. The measured error in temperatures from $B - V$ is estimated to be about ±96K according to Alonso et al. (1999). Since all our samples are located within the distance of 50 pc, the interstellar reddening can be neglected. In this case, we can use the uncorrected $B - V$, $b - y$ and $V - K$ colour indices, which will not cause any significant error. Fig. 3 compares the temperatures derived from different colour indices. Fig. 3(a) shows the comparison between effective temperatures from $B - V$ and those from $b - y$, and Fig. 3(b) shows comparison of effective temperatures from $V - K$ with those from $b - y$. Taking account of temperatures derived from $b - y$ shows that our choice is comparatively accurate. We can see from Fig. 3 that the temperature scatter derived from $B - V$ versus $b - y$ is smaller than that of $V - K$ versus $b - y$. The agreement between the effective temperatures deduced from $b - y$ and $B - V$ is quite good, the mean difference $\langle\, T(b-y) - T(B-V)\rangle$ amounting to 36 K, with an rms scatter of 48 K.

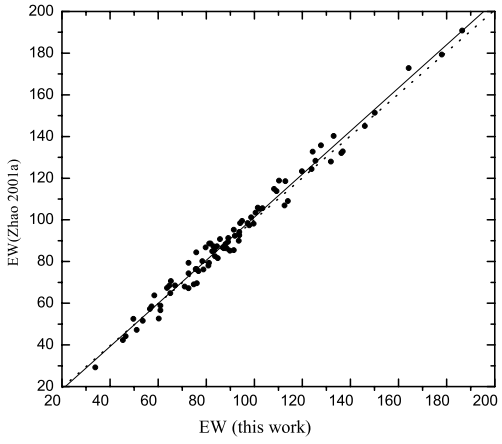

Figure 2. A comparison of our EWs (mÅ) with those of Zhao et al. (2001a) for the star HIP 3455. The solid line is a linear fit to the points, whereas the dotted line is the one-to-one relation.

Table 2 gives the temperatures derived from $B - V$, $b - y$ and $V - K$, namely $T(B - V)$, $T(b - y)$ and $T(V - K)$, respectively, where $V - K$ are taken from 2MASS[2] (have been making system transformations), $b - y$ from Hauck & Mermilliod (1998) and $B - V$ from SIMBAD.[3]

In order to check the photometric temperature, the excitation equilibrium was traced by studying the derived abundance from

[1] This publication makes use of data obtained from 2MASS, which is a joint project of the University of Massachusetts and the Infrared Processing and Analysis Centre/California Institute of Technology, funded by the National Aeronautics and Space Administration and the National Science Foundation.
[2] http://vizier.u-strasbg.fr/cgi-bin/VizieR?-source=II/246.
[3] http://simbad.u-strasbg.fr/sim-fid.pl.

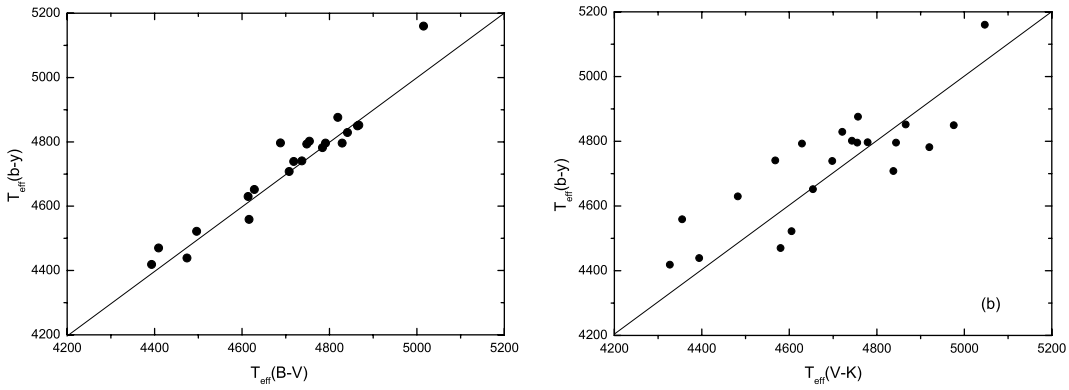

Figure 3. Comparison of effective temperatures derived from different photometric colour indices. (a): effective temperature derived from $B - V$ versus that from $b - y$. (b): effective temperature derived from $V - K$ versus that from $b - y$.

individual lines as a function of excitation potential. A linear least-squares fit to the abundance derived from each line versus low excitation potential is presented by the formula $[\mathrm{Fe/H}] = a + b\,\chi_{\mathrm{low}}$. The mean slope coefficient, b, is 0.005 ± 0.010 for all samples except for the five stars HIP 18199, HIP 76664, HIP 80000, HIP 93683 and HIP 99570 with b as high as 0.06, indicating that the adopted temperature matches the excitation equilibrium quite well for most of our sample.

3.2 Surface gravity

Before the launch of the *Hipparcos* satellite, the most popular method to determine the surface gravity was to force the abundances of different ionization stages of an element (usually Fe) to a consistent mean value. However, this procedure is affected by several uncertainties, including temperature structure, non-local thermodynamic equilibrium (NLTE) effects, and only a few available Fe II lines, etc. Therefore, the error in such a determination is often as high as 0.2–0.3 dex. With the release of the *Hipparcos* data, highly accurate parallaxes of the nearby stars are available. For those stars, the more accurate method is to determine the surface gravity by the relations of

$$\log \frac{g}{g_{\odot}} = \log \frac{M}{\mathrm{M}_{\odot}} + 4 \log \frac{T_{\mathrm{eff}}}{T_{\mathrm{eff},\odot}} + 0.4(M_{\mathrm{bol}} - M_{\mathrm{bol},\odot}), \qquad (1)$$

and

$$M_{\mathrm{bol}} = V_{\mathrm{mag}} + \mathrm{BC} + 5 \log \pi + 5, \qquad (2)$$

where M is the stellar mass, M_{bol} is the absolute bolometric magnitude, BC is the bolometric correction, and π is the parallax, taken from the *Hipparcos* catalogue (ESA 1997) with a measured accuracy better than 10 per cent. The bolometric correction is derived from the relation of Alonso et al. (1999) depending on temperature and metallicity. The stellar mass is estimated from the stars ' positions in the $M_v - \log T_{\mathrm{eff}}$ diagram by interpolating in the evolutionary tracks of Yonsei–Yale (Yi, Kim & Demarque 2003). These isochrones had been proved reasonably accurate by many high-quality observational data, and it can be used for stars from the stage of the pre-main-sequence birthline to the helium-core flash. For this method, the estimated error in surface gravity is about 0.1 dex, which will cause the stellar masses to increase by a factor of up to 1.26. For comparison, we also estimated the masses using the evolutionary tracks of Girardi et al. (2000). The difference in stellar masses from the two sets of evolutionary tracks is less than $0.3\,\mathrm{M}_{\odot}$.

When surface gravity is determined through *Hipparcos* parallaxes, iron abundances derived from Fe I are well consistent with those from Fe II (see Fig. 4) in our sample. The deviation is less than 0.1 dex for most stars with a mean value of 0.01 ± 0.05 dex.

3.3 Metal abundances

The initial metal abundances for some stars were taken from the literature (Geisler, Clariá & Minniti 1991; Cayrel de Strobel et al. 1997; Tautvaišienė 1997; Taylor 1999; Zhao, Qiu & Mao 2001c; Kubiak et al. 2002). For the stars whose metal abundances had not been determined in former work, we used the initial value of $[\mathrm{Fe/H}] = 0.0$. The element abundance is obtained from each line by forcing the computed EW to agree with the measured one. The iron abundance was taken as a representative of the mean metallicity and all abundances were scaled accordingly from the solar composition, which were calculated from the Moon spectrum. The Moon spectrum was taken in the Coudé Echelle Spectrograph (CES) attached to 2.16-m telescope of the National Astronomical Observatories (Xinglong, China, see Zhao & Li 2001, for details), since we did not take it at FEROS and regarding that there is no big difference between these two systems by comparison of the EWs of common star HIP 3455 (see Fig. 2). Considering that the input [Fe/H] and the spectroscopic value may be quite different, the whole procedure of determination of T_{eff}, $\log g$ and metallicity was repeated until the final metallicity from the EW calculation was fully consistent with input [Fe/H] within 0.03 dex.

3.4 Microturbulence velocity

Microturbulent velocities were determined by requiring a zero slope of [Fe/H] versus their EWs, and it is determined in the same way for the Moon spectrum. We applied this calculation to the Fe I lines with $10 < \mathrm{EW} < 100$ mÅ. The mean value for our sample amounts to 1.37, with a scatter of $0.09\ \mathrm{km\,s^{-1}}$.

For our sample stars, the temperatures range from 4375 to 5050 K while surface gravity spans from 2.29 to 2.94 and mass coverage is from 1.2 to $2.8\,\mathrm{M}_{\odot}$. Table 3 gives the basic stellar atmospheric parameters for 63 nearby red clump giants. The successive columns present the star name, absolute magnitude, effective temperature, surface gravity, input metallicity, microturbulence velocity, stellar initial mass, parallax, parallax error, bolometric correction, and final iron abundance. Finally, the uncertainties of parameters are: $\sigma(T_{\mathrm{eff}}) = 100\,\mathrm{K}, \sigma([\mathrm{Fe/H}]) = 0.1, \sigma([\mathrm{Fe/H}]) = 0.1$ and $\sigma([\xi_{\mathrm{t}}]) = 0.2$.

Table 2. The effective temperatures derived from different colour indices.

Star	HIP	$T(B-V)$	$T(b-y)$	$T(V-K)$
HD 360	671	4741.	–	4828.
HD 770	966	4696.	–	4724.
HD 3750	3137	4560.	–	4554.
HD 4188	3455	4777.	–	4873.
HD 4211	3456	4616.	4559.	4355.
HD 5268	4257	4864.	4850.	4976.
HD 5722	4587	4865.	–	4859.
HD 6559	5170	4706.	–	4720.
HD 6976	5485	4791.	4796.	4755.
HD 8651	6592	4708.	4708.	4838.
HD 9362	7083	4754.	4802.	4743.
HD 10042	7271	4808.	–	4808.
HD 10142	7643	4688.	4797.	4779.
HD 10537	7955	4707.	–	4753.
HD 11643	8820	4565.	–	4547.
HD 15471	11524	4618.	–	4713.
HD 15779	11791	4784.	4782.	4920.
HD 16815	12486	4732.	–	4477.
HD 16975	12608	5015.	5160.	5047.
HD 17652	13147	4790.	–	4695.
HD 17824	13288	4987.	–	4807.
HD 24706	18199	4393.	4419.	4327.
HD 25170	18401	4610.	–	4651.
HD 26967	19747	4614.	4630.	4482.
HD 120452	67494	4715.	–	4716.
HD 138289	76532	4672.	–	4715.
HD 139254	76664	4434.	–	4376.
HD 140573	77070	4496.	4522.	4605.
HD 141680	77578	4735.	–	4765.
HD 142198	77853	4718.	4739.	4698.
HD 143546	78639	4977.	–	4843.
HD 143787	78650	4375.	–	4383.
HD 144046	78685	4913.	–	4846.
HD 146388	79666	4603.	–	4622.
HD 146791	79882	4861.	–	4985.
HD 146686	80000	4699.	–	4618.
HD 147700	80343	4748.	4793.	4629.
HD 149324	81852	4677.	–	4616.
HD 159433	86170	4596.	–	4706.
HD 160315	86391	4829.	4796.	4844.
HD 166464	89153	4716.	–	4712.
HD 167768	89587	4856.	–	4957.
HD 169916	90496	4689.	–	4584.
HD 169767	90568	4720.	4439.	4750.
HD 176704	93498	4474.	–	4394.
HD 177241	93683	4759.	–	4876.
HD 177873	94005	4627.	4852.	4573.
HD 189561	98575	4867.	–	4866.
HD 188887	98624	4434.	4470.	4416.
HD 191584	99570	4409.	–	4580.
HD 196171	101772	4788.	–	4653.
HD 204381	106039	5050.	4652.	4824.
HD 214122	111600	4628.	4741.	4654.
HD 215104	112203	4737.	4829.	4568.
HD 216763	113246	4841.	–	4721.
HD 219449	114855	4601.	4876.	4494.
HD 219615	114971	4819.	–	4757.
HD 219784	115102	4552.	–	4426.
HD 220572	115620	4706.	–	4753.
HD 220954	115830	4696.	–	4660.
HD 221115	115919	4973.	–	4975.
HD 222493	116853	4901.	–	4816.
HD 223252	117375	4952	–	4802

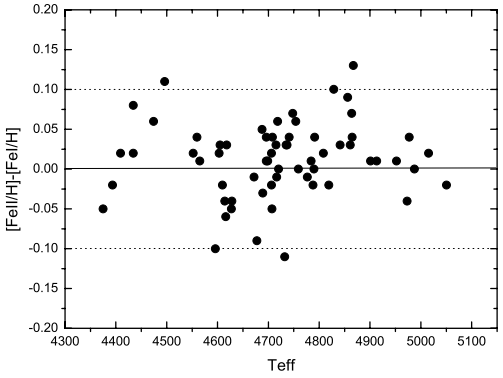

Figure 4. Difference in iron abundances derived from Fe I and Fe II lines versus effective temperature.

3.5 Consistency check of atmospheric parameters

To check the stellar atmospheric parameters adopted here, we compared our results for 22 stars in common with those of McWilliam (1990, hereafter McW90), and for two stars in common with those of Mishenina et al. (2006).

(i) *Comparision with McWilliam (1990)*. McW90 analysed 671 GK giant spectra and gave their stellar atmospheric parameters and absolute abundances for some lines of Si, Ca, Sc, Ti, V, Co, Ni, Sr, Zr, Y, La, Nd and Eu. Unfortunately, they did not estimate the abundance zero-point errors and there was a large line-to-line spread for some elements; therefore, only stellar atmospheric parameters were taken to compare with their work. We list the detailed comparative results in Table 4. The successive columns are: star name, effective temperature, surface gravity, metallicity, microturbulence velocity of our work and that of McW90, and the difference of these four parameters between our results and that of McW90. McW90 derived effective temperatures with empirical and semi-empirical methods, involving a relation between colour and effective temperature. The difference between two sets of data on effective temperature is less than 100 K, with a standard deviation of 54 K, except for the stars HIP 113246 and HIP 115102, for which the difference is 211 and 122 K, respectively. Such a diversity in effective temperatures for most of the 22 stars can cause less than 0.04-dex difference in metallicity. For HIP 113246 and HIP 115102, it will cause about 0.1- and 0.06-dex difference in metallicity, respectively. Fig. 5(a) shows comparison between effective temperatures, and Fig. 5(b) shows comparison between metallicities.

The surface gravity in McW90 was determined using equation (1). However, the method to obtain the stellar mass and bolometric correction was different. Most of the differences in our respective surface gravities are less than 0.2 dex, except that three stars are higher in $\log g$ by more than 0.3 dex and five are between 0.2 and 0.3 dex higher. The scatter of 0.2 dex in surface gravities would induce differences less than 0.02 dex in metallicity.

The differences between microturbulence velocities are significant, typically around 0.8 km s^{-1}, which will induce differences of 0.2 dex in metallicity. The method to derive microturbulence velocity in McW90 is the same as ours, such diversity may be due to their narrow spectral coverage and the few Fe I lines available. From Fig. 5(b), we note that there is a systematic deviation of 0.1–0.2 dex between the two sets of metallicity. This offset may be explained by the following two reasons: one is that McW90 assumed a solar metallicity of [Fe/H] = 7.67 (Grevesse 1984), while we take it as [Fe/H] = 7.60 (derived from Moon spectrum, which will be

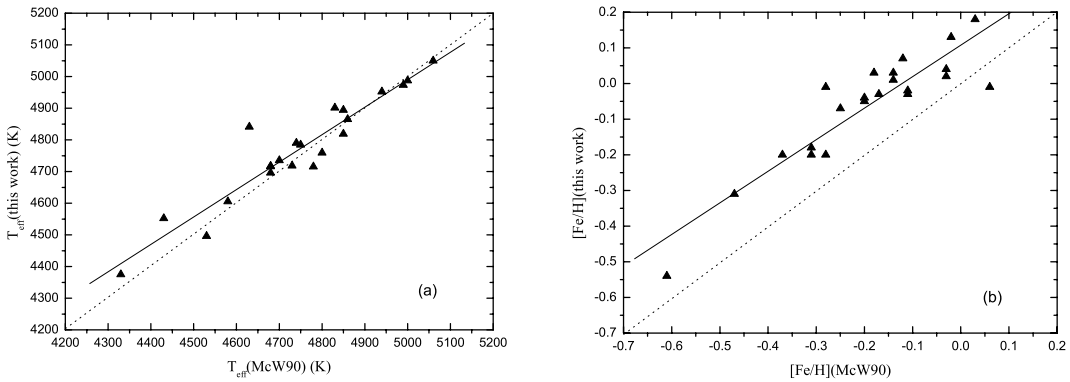

Figure 5. (a): comparison of our effective temperatures with those of McW90. (b): comparison of metallicity results with those of McW90. The filled triangles represent the 22 stars in common. The dotted line shows the one-to-one relation, and the solid line is the linear fit to data.

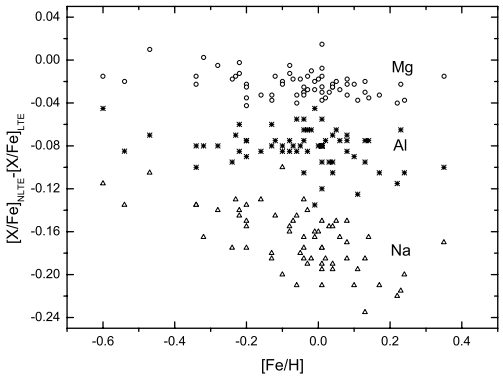

Figure 6. Difference of element abundance ratios calculated under NLTE and LTE assumptions for Mg, Na and Al, respectively.

explained in Section 6.1), and another is the systematic difference of microturbulence velocities.

(ii) *Comparison with Mishenina et al.* (*2006*). Mishenina et al. (2006) analysed elemental abundances for 177 red clump giants. Table 5 gives the comparison of stellar parameters of Mishenina et al. (2006) with ours for two common stars. The consequence columns are star name, effective temperature, surface gravity, metallicity, microturbulence velocity for our results and those of Mishenina et al. (2006). From Table 5, we can conclude that our stellar parameters are consistent with those of Mishenina et al. (2006) very well, although different methods were used.

4 ATOMIC-LINE DATA

We adopted the flux-constant, homogeneous and LTE model atmospheres given by Kurucz (1993) for abundance determination of O, Ca, Si, Ti, Ni, V and Ba. Accurate oscillator strengths (*gf* values) are required in abundance determinations from high-resolution, high-S/N stellar spectra.

We take most of the Fe I lines from table 4 of Chen et al. (2000, hereafter Chen00). To increase the accuracy of the microturbulence velocities, some weak lines are necessary for analysis. Therefore, we selected some weak lines from the solar table line. For those lines, the $\log gf$ are taken from Blackwell et al. (1982a,b), O'Brian et al. (1991), Bard, Kock & Kock (1991) and Bard & Kock (1994). We use eight Fe II lines for calculation, five of them are taken from chen00, and the other three, $\lambda\lambda$ 5414.075, 5425.259 and 6369.462, are taken from Gehren et al. (2001). For the other elements we adopt the $\log gf$ values from Chen00 (see references therein). All atomic-line data used and EW values of programme stars are shown in Table 1 (in the electronic version of this paper on *Synergy* – see the Supplementary Material section).

5 ABUNDANCE AND THEIR UNCERTAINTIES

5.1 Uncertainties of the abundance

The abundance errors mainly arise from two parts: the systematic errors introduced by the atmospheric parameters, and random errors including errors in determining EW, oscillator strengths, and damping constants. For our sample, the typical uncertainty of the EW is about 4 mÅ which corresponds to a change in derived abundances less than 0.10 dex. Table 6 shows the effects on the abundances due to changes of 4 mÅ in EW, 100 K in effective temperature, 0.1 dex in surface gravity, 0.1 dex in metallicity, 0.2 km s^{-1} in microturbulent velocity, and the overall uncertainty corresponding to the combined effect of the likely uncertainties in all these quantities for a typical star, HIP 101772. Finally, we take the overall uncertainty as the adopted uncertainty in abundance determination. We can see that the abundances relative to iron are not quite sensitive to the variations in the atmospheric parameters, with an exception of [O/Fe], which is well known to be strongly dependent on temperature. Since lines in our sample are stronger than in disc stars, the effects of microturbulence velocity are also more important than in disc stars (e.g. Chen00).

5.2 NLTE abundance of sodium, magnesium and aluminum

For Na, Mg and Al, the abundance results are derived from NLTE calculations. The abundance determinations are carried out using a spectral synthesis method based on the IDL/FORTRAN SIU software package by Reetz (private communication). The synthetic spectra are convolved with macroturbulence, rotational and instrumental broadening profiles in order to match the observed line profiles. Na and Al abundances are obtained with a best fit to the observed line profiles. Two lines of Na (6154/6160 Å) and Al (7835/7836 Å) were considered here, while four lines were used to determine the Mg abundances (4571, 4702, 5528 and 5711 Å). The oscillator strengths and collisional broadening parameters describing van der Waals interaction with hydrogen atoms are taken from Gehren et al. (2004). The NLTE effect of -0.10 to -0.24 with a mean value of -0.17 for Na, -0.05 to 0.02 for Mg with a mean value of -0.02, and

Table 3. The basic stellar parameters of 63 nearby red clump giants.

Star	V	M_v	$T_{\rm eff}$ (K)	$\log g$	[M/H]	$\xi_{\rm t}$ (km s^{-1})	Mass ($M_\odot$)	π (mas)	$\delta(\pi)$	BC	[Fe/H]
HD 360	5.992	0.946	4741	2.73	−0.05	1.3	1.91	9.79	0.92	−0.361	−0.07
HD 770	6.529	1.036	4696	2.68	−0.10	1.4	1.67	7.97	0.79	−0.382	−0.12
HD 3750	6.005	1.162	4560	2.60	0.06	1.5	1.51	10.75	0.71	−0.454	0.03
HD 4188	4.775	0.732	4777	2.71	−0.05	1.5	2.17	15.54	0.82	−0.334	−0.08
HD 4211	5.960	0.673	4616	2.53	0.00	1.4	1.84	8.76	0.72	−0.419	−0.01
HD 5268	6.162	0.835	4864	2.63	−0.47	1.4	1.48	8.60	0.79	−0.312	−0.46
HD 5722	5.621	0.696	4865	2.75	−0.20	1.4	2.20	10.35	0.96	−0.310	−0.22
HD 6559	6.125	0.970	4706	2.71	0.02	1.4	1.87	9.31	0.90	−0.378	0.02
HD 6976	6.399	1.156	4791	2.87	0.10	1.3	2.06	8.94	0.83	−0.339	0.08
HD 8651	5.427	1.033	4708	2.67	−0.16	1.4	1.63	13.22	0.64	−0.376	−0.18
HD 9362	3.949	0.675	4754	2.61	−0.26	1.3	1.84	22.15	0.61	−0.355	−0.28
HD 10042	6.115	0.461	4808	2.59	−0.32	1.5	2.00	7.40	0.52	−0.333	−0.34
HD 10142	5.943	0.965	4688	2.65	−0.08	1.4	1.69	10.10	0.68	−0.386	−0.10
HD 10537	5.263	1.147	4707	2.69	−0.20	1.2	1.52	15.02	0.72	−0.377	−0.22
HD 11643	6.095	0.772	4565	2.51	0.05	1.5	1.73	8.62	0.72	−0.450	0.04
HD 15471	6.113	0.835	4618	2.60	0.06	1.4	1.87	8.80	0.70	−0.418	0.04
HD 15779	5.364	0.808	4784	2.75	−0.01	1.4	2.16	12.27	1.13	−0.342	−0.05
HD 16815	4.124	0.877	4732	2.60	−0.32	1.3	1.53	22.42	0.57	−0.365	−0.33
HD 16975	5.999	0.669	5015	2.91	0.04	1.3	2.71	8.59	0.62	−0.255	0.01
HD 17652	4.465	0.894	4790	2.67	−0.31	1.4	1.65	19.31	0.67	−0.340	−0.34
HD 17824	4.750	1.008	4987	2.97	0.00	1.2	2.38	17.85	0.69	−0.265	−0.03
HD 24706	5.927	0.712	4393	2.36	0.15	1.3	1.67	9.06	0.56	−0.569	0.13
HD 25170	6.144	0.864	4610	2.55	−0.08	1.4	1.61	8.79	0.50	−0.422	−0.10
HD 26967	3.860	1.084	4614	2.62	−0.01	1.2	1.55	27.85	0.51	−0.420	−0.02
HD 120452	4.970	0.618	4715	2.63	0.02	1.4	2.13	13.48	0.72	−0.373	0.01
HD 138289	5.796	1.186	4672	2.71	−0.02	1.3	1.59	11.97	1.03	−0.386	−0.04
HD 139254	6.199	1.113	4434	2.51	0.25	1.4	1.55	9.61	0.59	−0.542	0.24
HD 140573	2.638	0.882	4496	2.52	0.18	1.5	1.79	44.54	0.71	−0.497	0.17
HD 141680	5.230	0.697	4735	2.62	−0.20	1.4	1.88	12.40	0.73	−0.364	−0.20
HD 142198	4.136	0.665	4718	2.58	−0.20	1.4	1.84	20.22	0.88	−0.372	−0.23
HD 143546	4.648	0.524	4977	2.84	−0.02	1.3	2.78	14.97	0.76	−0.268	−0.05
HD 143787	4.973	0.909	4375	2.29	0.03	1.3	1.21	15.39	0.91	−0.580	0.01
HD 144046	6.076	0.690	4913	2.83	0.01	1.4	2.52	8.37	0.82	−0.291	0.01
HD 146388	5.714	0.780	4603	2.61	0.14	1.4	2.03	10.31	0.73	−0.428	0.13
HD 146791	3.240	0.650	4861	2.77	−0.07	1.4	2.39	30.34	0.79	−0.311	−0.08
HD 146686	4.017	1.057	4699	2.80	0.25	1.3	2.16	25.58	0.86	−0.382	0.23
HD 147700	4.491	0.806	4748	2.68	−0.11	1.4	1.94	18.32	0.89	−0.358	−0.13
HD 149324	4.240	0.819	4677	2.63	−0.05	1.3	1.84	20.69	0.51	−0.384	−0.05
HD 159433	4.272	1.047	4596	2.52	−0.22	1.2	1.30	22.64	0.94	−0.430	−0.25
HD 160315	6.262	0.889	4829	2.86	0.14	1.2	2.47	8.42	0.83	−0.323	0.14
HD 166464	4.980	0.608	4716	2.65	0.03	1.3	2.24	13.35	0.81	−0.373	0.00
HD 167768	6.000	0.958	4856	2.60	−0.62	1.4	1.24	9.81	0.83	−0.316	−0.60
HD 169916	2.833	0.960	4689	2.66	−0.04	1.2	1.73	42.20	0.90	−0.386	−0.06
HD 169767	4.130	1.171	4720	2.71	−0.18	1.2	1.53	25.60	0.78	−0.371	−0.20
HD 176704	5.640	1.001	4474	2.56	0.36	1.2	1.81	11.81	0.77	−0.516	0.36
HD 177241	3.771	0.625	4759	2.66	−0.03	1.4	2.14	23.49	0.78	−0.353	−0.04
HD 177873	4.582	0.937	4627	2.59	−0.01	1.3	1.64	18.67	0.83	−0.412	0.01
HD 189561	6.018	1.107	4867	2.91	0.01	1.2	2.15	10.42	0.78	−0.308	0.04
HD 188887	5.335	1.052	4434	2.45	0.13	1.5	1.40	13.91	0.66	−0.539	0.11
HD 191584	6.221	1.105	4409	2.49	0.23	1.4	1.40	9.48	0.89	−0.559	0.22
HD 196171	3.116	0.656	4788	2.69	−0.11	1.5	2.13	32.21	0.75	−0.340	−0.13
HD 204381	4.513	0.811	5050	2.96	−0.01	1.2	2.59	18.18	0.89	−0.245	−0.01
HD 214122	5.821	0.917	4628	2.59	−0.01	1.3	1.65	10.45	0.89	−0.412	−0.03
HD 215104	4.847	0.685	4737	2.62	−0.19	1.5	1.91	14.71	0.76	−0.363	−0.20
HD 216763	4.226	0.636	4841	2.72	−0.20	1.4	2.20	19.14	0.87	−0.319	−0.21
HD 219449	4.210	0.919	4605	2.59	0.01	1.4	1.72	21.97	0.89	−0.426	0.01
HD 219615	3.690	0.673	4819	2.53	−0.54	1.3	1.43	24.92	0.89	−0.330	−0.54
HD 219784	4.415	0.720	4552	2.45	−0.05	1.4	1.60	18.24	0.80	−0.457	−0.06
HD 220572	5.602	0.891	4706	2.73	0.10	1.4	2.12	11.42	0.60	−0.378	0.08
HD 220954	4.280	0.843	4696	2.70	0.07	1.5	2.09	20.54	0.8	−0.382	0.06
HD 221115	4.549	0.866	4973	2.94	0.04	1.4	2.53	18.34	0.74	−0.269	0.05
HD 222493	5.898	0.571	4901	2.83	0.13	1.3	2.80	8.60	0.86	−0.295	0.10
HD 223252	5.509	0.753	4952	2.88	−0.02	1.4	2.51	11.19	0.85	−0.277	−0.04

Table 4. The comparison of stellar parameters of 22 stars common with the sample of McW90.

Star	$T_{\rm eff}$	$T_{\rm eff_{Mc}}$	$\log g$	$\log g_{\rm Mc}$	[Fe/H]	[Fe/H]$_{\rm Mc}$	$\xi_{\rm t}$	$\xi_{\rm t_{Mc}}$	$\delta\, T_{\rm eff}$	$\delta \log g$	δ[Fe/H]	$\delta\xi_{\rm t}$
HD 5722	4865	4860	2.75	2.89	−0.20	−0.37	1.4	2.2	5	−0.14	0.17	−0.8
HD 15779	4784	4750	2.75	2.85	−0.01	0.06	1.4	2.1	34	−0.10	−0.07	−0.7
HD 17652	4790	4740	2.67	2.90	−0.31	−0.47	1.4	2.3	50	−0.23	0.16	−0.9
HD 17824	4987	5000	2.97	3.18	−0.03	−0.17	1.2	2.0	−13	−0.21	0.14	−0.8
HD 120452	4715	4780	2.63	2.80	0.02	−0.03	1.4	2.2	−65	−0.17	0.05	−0.8
HD 140573	4496	4530	2.52	2.76	0.18	0.03	1.5	2.3	−34	−0.24	0.15	−0.8
HD 141680	4735	4700	2.62	3.02	−0.20	−0.28	1.4	2.0	35	−0.40	0.08	−0.6
HD 142198	4718	4730	2.58	2.99	−0.18	−0.31	1.4	2.2	−12	−0.41	0.13	−0.8
HD 143787	4375	4330	2.29	2.23	0.03	−0.14	1.3	2.1	45	0.06	0.17	−0.8
HD 146791	4894	4850	2.77	3.03	−0.07	−0.25	1.4	2.2	44	−0.26	0.18	−0.8
HD 166464	4716	4680	2.65	2.76	0.03	−0.18	1.3	2.1	36	−0.11	0.21	−0.8
HD 169916	4717	4680	2.66	2.95	−0.04	−0.20	1.2	1.7	37	−0.29	0.16	−0.5
HD 177241	4759	4800	2.66	3.03	−0.03	−0.11	1.4	2.1	−41	−0.37	0.08	−0.7
HD 204381	5050	5060	2.96	3.01	−0.01	−0.28	1.2	2.0	−10	−0.05	0.27	−0.8
HD 216763	4841	4630	2.72	2.76	−0.20	−0.31	1.4	1.6	211	−0.04	0.11	−0.2
HD 219449	4605	4580	2.59	2.69	0.01	−0.14	1.4	2.1	25	−0.10	0.15	−0.7
HD 219615	4819	4850	2.53	3.04	−0.54	−0.61	1.3	2.4	−31	−0.51	0.07	−1.1
HD 219784	4552	4430	2.45	2.52	−0.05	−0.2	1.4	2.1	122	−0.07	0.15	−0.7
HD 220954	4696	4680	2.70	2.78	0.07	−0.12	1.5	2.3	16	−0.08	0.19	−0.8
HD 221115	4973	4990	2.94	2.91	0.04	−0.03	1.5	2.0	−17	0.03	0.07	−0.5
HD 222493	4901	4830	2.83	2.81	0.13	−0.02	1.3	2.1	71	0.02	0.15	−0.8
HD 223252	4952	4940	2.88	2.97	−0.02	−0.11	1.4	1.9	12	−0.09	0.09	−0.5

Table 5. The comparison of stellar parameters of two stars common with the sample of Mishenina et al. (2006).

Star	$T_{\rm eff}$	$T_{\rm eff_{Mi}}$	$\log g$	$\log g_{\rm Mi}$	[Fe/H]	[Fe/H]$_{\rm Mi}$	$\xi_{\rm t}$	$\xi_{\rm t_{Mi}}$
HD 4188	4777	4809	2.71	2.70	−0.05	0.04	1.5	1.5
HD 15779	4784	4821	2.75	2.70	−0.01	0.02	1.4	1.5

Table 6. The estimation errors for an abundance analysis.

	$(\sigma_{\rm EW}/\sqrt{N})$	$\Delta T_{\rm eff}$ +100	$\Delta\log g$ +0.1	Δ[Fe/H] +0.1	$\Delta\xi_{\rm t}$ +0.2	$\sigma_{\rm tot}$
Δ[Fe I/H]	0.01	+0.05	+0.01	+0.01	−0.07	0.09
Δ[Fe II/H]	0.02	−0.09	+0.06	+0.04	−0.05	0.13
Δ[O/Fe]	0.06	−0.20	+0.03	−0.01	+0.05	0.22
Δ[Si/Fe]	0.02	−0.07	+0.01	+0.01	+0.04	0.08
Δ[Ca/Fe]	0.02	+0.06	−0.02	+0.05	−0.02	0.09
Δ[Ti/Fe]	0.03	+0.09	−0.01	+0.00	+0.01	0.10
Δ[V/Fe]	0.03	+0.11	−0.01	+0.03	+0.01	0.12
Δ[Ni/Fe]	0.01	−0.01	+0.00	+0.00	−0.03	0.03
Δ[Ba/Fe]	0.03	−0.02	+0.01	+0.03	+0.09	0.10

Note. HIP 101772: $T_{\rm eff}$ = 4788K, $\log g$ = 2.69, [Fe/H] = −0.11, $\xi_{\rm t}$ = 1.5 km s^{-1}.

−0.05 to −0.14 with a mean value of −0.08 for Al is presented in Fig. 11. The NLTE analysis for Mg is very well consistent with that of Zhao & Gehren (2000), which suggested that the NLTE effect is within 0.05 dex for cool giants. However, the NLTE effect for Na is larger than that in Mishenina et al. (2006), which shows a correction of 0.10–0.15. Table 7 shows the abundance determined by LTE and NLTE analyses for Na, Mg and Al. The final abundance scatter of single lines is between 0 and 0.04 for [Na/Fe] in individual stars with a mean value of $\langle\sigma$[Na/Fe]$\rangle = 0.009 \pm 0.010$ for all stars. For [Mg/Fe] and [Al/Fe], the corresponding values are 0.01–0.06 and 0–0.05 for individual stars with $\langle\sigma$[Mg/Fe]$\rangle = 0.020 \pm 0.011$ and $\langle\,\sigma$[Mg/Fe]$\rangle = 0.015 \pm 0.010$ for all stars.

The atomic models of Na, Mg and Al employed in this paper are described by Gehren et al. (2004) and Shi, Gehren & Zhao (2004). The atom contains 58 levels of Na I (Al I) and the ground state of Na II (Al II), while the atomic model of Mg consists of 85 levels: 84 levels of Mg I and the ground state of Mg II. All bound–free radiative cross-sections have been included from close-coupling calculations of Butler (in preparation) and Butler, Mendoza & Zeippen (1993). The cross-sections for excitation and de-excitation due to collisions with neutral hydrogen are taken from Drawin (1968, 1969); we adopt a scaling factor of 0.05 for Na and Mg, whereas 0.002 for Al.

6 RESULTS AND DISCUSSIONS

In this section, we present the abundance trends for 10 elements based on our spectral analysis. To see the difference in the abundance pattern from that of disc stars, we compare our LTE results for Ca, Si, Ti, Ni and Ba, in Fig. 7, with the abundance ratios of (hereafter Edvardsson93 Edvardsson et al. 1993) as the most classical work on disc stars. In Fig. 8, we present our LTE results for Ca, Si, Ti, Ni, V and Ba, together with the abundance ratios of Chen00. Since we used the same methods to determine stellar atmospheric parameters and selected almost the same lines and $\log gf$ values, that comparison should show the true difference between the two groups of stars in different stages of evolution.

6.1 Iron abundance

The iron lines we used for abundance determination are weak and intermediate to strong lines with EWs between 10 and 100 mÅ since weaker lines would lead to increased random errors and possibly systematic abundance overestimates. On the other hand, stronger lines are very sensitive to the microturbulence and damping constants, which cause the large error in abundance determinations. Finally, 40–100 iron lines were selected to determine the iron abundance.

Table 7. The abundance determined by LTE and NLTE analyses for Na, Mg and Al of 63 nearby red clump giants relative to Fe.

HD	[Mg/Fe]		[Na/Fe]		[Al/Fe]	
	LTE	NLTE	LTE	NLTE	LTE	NLTE
HD 360	0.05	0.04	0.12	−0.04	0.08	−0.01
HD 770	0.06	0.05	0.13	−0.02	0.09	0.01
HD 3750	0.07	0.04	0.17	0.02	0.08	−0.02
HD 4188	0.04	0.03	0.18	0.02	0.09	0.00
HD 4211	0.19	0.16	0.23	0.07	0.33	0.20
HD 5268	0.20	0.21	−0.06	−0.16	0.16	0.09
HD 5722	0.16	0.15	0.10	−0.04	0.07	0.01
HD 6559	0.16	0.13	0.30	0.11	0.15	0.08
HD 6976	0.07	0.03	0.17	0.02	0.02	−0.06
HD 8651	0.19	0.16	0.08	−0.05	0.13	0.04
HD 9362	0.20	0.19	0.10	−0.05	0.12	0.04
HD 10042	0.37	0.34	0.09	−0.05	0.11	0.03
HD 10142	0.18	0.16	0.12	0.02	0.11	0.03
HD 10537	0.22	0.21	0.18	0.04	0.10	0.02
HD 11643	0.23	0.20	0.24	0.09	0.16	0.06
HD 15471	0.19	0.17	0.34	0.14	0.19	0.09
HD 15779	0.16	0.14	0.23	0.05	0.07	−0.02
HD 16815	0.24	0.24	0.19	0.02	0.17	0.09
HD 16975	0.08	0.10	0.22	0.07	−0.04	−0.10
HD 17652	0.21	0.20	0.06	−0.08	0.21	0.11
HD 17824	0.01	−0.01	0.20	0.06	0.04	−0.03
HD 24706	0.16	0.13	0.38	0.15	0.18	0.09
HD 25170	0.17	0.15	0.27	0.07	0.14	0.05
HD 26967	0.14	0.13	0.19	0.00	0.07	0.00
HD 120452	0.04	0.03	0.27	0.06	0.07	−0.02
HD 138289	0.05	0.02	0.13	−0.01	0.03	−0.04
HD 139254	0.09	0.05	0.34	0.14	0.20	0.10
HD 140573	0.08	0.05	0.35	0.14	0.20	0.09
HD 141680	0.18	0.15	0.12	−0.02	0.13	0.04
HD 142198	0.30	0.28	0.08	−0.05	0.08	0.01
HD 143546	0.09	0.07	0.29	0.12	0.17	0.09
HD 143787	0.21	0.18	0.21	0.03	0.21	0.09
HD 144046	0.06	0.05	0.32	0.13	−0.01	−0.09
HD 146388	0.15	0.13	0.19	0.00	0.01	−0.07
HD 146791	0.13	0.12	0.12	−0.04	0.00	−0.08
HD 146686	0.14	0.11	0.33	0.11	0.08	0.02
HD 147700	0.13	0.10	0.23	0.05	0.08	0.02
HD 149324	0.26	0.23	0.21	0.03	0.14	0.04
HD 159433	0.22	0.20	0.08	−0.10	0.10	0.01
HD 160315	−0.01	−0.05	0.19	0.03	0.01	−0.07
HD 166464	0.05	0.03	0.09	−0.08	−0.01	−0.09
HD 167768	0.33	0.31	0.11	−0.01	0.21	0.16
HD 169916	0.11	0.08	0.10	−0.05	0.02	−0.04
HD 169767	0.16	0.14	0.17	−0.01	0.09	0.02
HD 176704	0.16	0.14	0.33	0.16	0.22	0.12
HD 177241	0.07	0.04	0.18	0.01	0.10	0.02
HD 177873	0.13	0.11	0.19	−0.01	0.12	0.04
HD 189561	0.01	−0.01	0.26	0.07	0.07	0.00
HD 188887	0.14	0.10	0.19	−0.01	0.23	0.10
HD 191584	0.21	0.17	0.37	0.15	0.24	0.12
HD 196171	0.09	0.06	0.19	0.01	0.11	0.03
HD 204381	−0.05	−0.07	0.19	0.03	−0.05	−0.10
HD 214122	0.12	0.09	0.20	0.01	0.10	0.02
HD 215104	0.10	0.06	0.15	−0.01	0.07	−0.01
HD 216763	0.08	0.04	0.10	−0.05	0.06	−0.02
HD 219449	0.14	0.10	0.10	−0.08	0.13	0.03
HD 219615	0.42	0.40	0.20	0.07	0.29	0.21
HD 219784	0.15	0.11	0.19	−0.03	0.11	0.03
HD 220572	0.07	0.05	0.15	−0.04	0.07	−0.01
HD 220954	0.10	0.08	0.18	0.01	0.13	0.06
HD 221115	0.01	−0.01	0.20	0.05	0.03	−0.04
HD 222493	0.04	0.02	0.37	0.16	0.07	−0.02
HD 223252	0.03	0.00	0.22	0.05	0.07	0.01

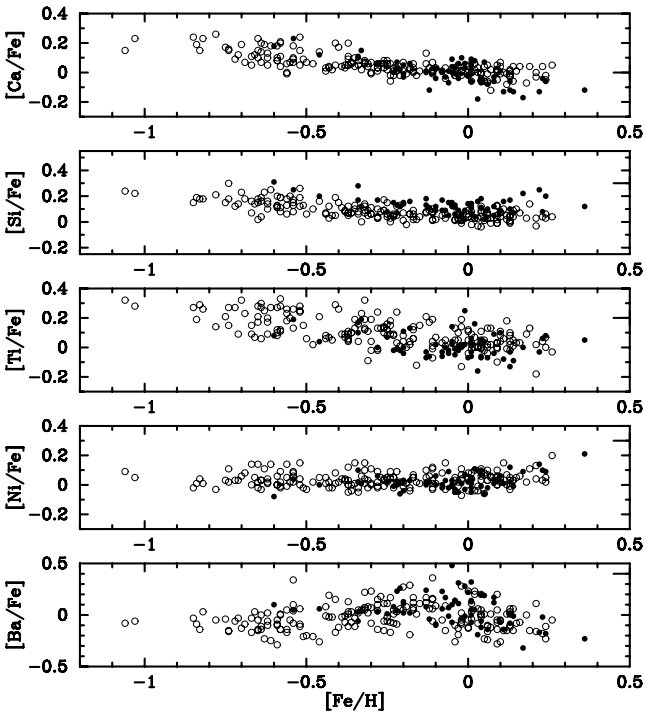

Figure 7. The LTE abundance pattern of Ca, Si, Ti, Ni and Ba for our 63 stars compared with that of Edvardsson93. The filled circles represent our results, and the open circles refer to the results of Edvardsson93.

Solar abundances were calculated from the Moon spectrum, which was utilized to derive stellar abundances relative to solar values. Table 8 shows the relative abundance ratio and adopted uncertainties of Ca, Si, Ti, Ni, V and Ba relative to Fe for our 63 nearby red clump giants.

6.2 Oxygen

Since oxygen is the third most abundant element except for H and He, determining oxygen abundances in different types of evolutionary stages is of great importance, not only for its role in stellar opacities and energy generation. It also provides a way to determine the time-scale of Galactic evolution and star formation rates, since the assumed initial oxygen abundance greatly affects the calculated stellar age (e.g. VandenBerg 1992). Oxygen is produced by SNe II, which will exhaust their life in a few million years and explode the products of nucleosynthesis, from C to Ni, leading to overabundances in the next generation of metal-poor stars for these elements. The forbidden line λ6300 is blended in our spectra; therefore, we derive the oxygen abundance from the O I λ7774 triplet lines, which are affected by NLTE effects and possibly also by convective inhomogeneities, as supported both theoretically and empirically (cf. Eriksson & Toft 1979; Nissen, Edvardsson & Gustafsson 1985; Kiselman 1991, 1993). Edvardsson93 found a correlation between oxygen abundances derived from [O I] λ6300 and those from infrared triplet, $[O/Fe]_{6300} = -0.078 + 0.6794[O/Fe]_{7774}$, which is also taken by Chen00 to scale the oxygen abundances obtained from the triplet to those of [O I] λ6300.

For our sample, the NLTE corrections according to the prescription of Gratton et al. (1999) are within an interval of 0.10–0.15 dex. However, the adopted neutral H collision rates in Gratton et al. (1999) are 30 times smaller than most investigators used, which

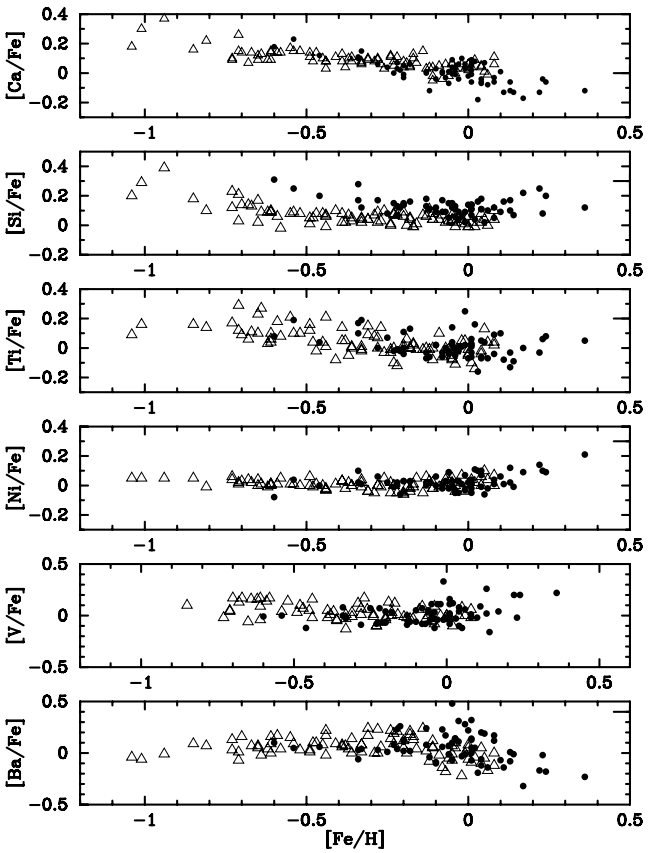

Figure 8. The LTE abundance pattern of Ca, Si, Ti, Ni and Ba for our 63 stars compared with that of Chen00. The filled circles represent our results, and the open triangles represent the results of Chen00.

cause underestimation of NLTE effect. Therefore, we take NLTE correction given by Takeda (2003). Table 9 gives the EWs, LTE abundance relative to H values for O triplet, their mean LTE [O/Fe] value, NLTE correction for O triplet and their NLTE [O/Fe] value. From Table 8, we can see that EW values for λ7774 are even larger than the line of λ7772 for some stars, which are also reproduced in Schuler et al. (2006), suggesting that λ7774 may be blending by Fe I line at λ7774 (Takeda, Kawanomoto & Sadakane 1998) in giants. Finally, the O abundances are taken as the mean values of λ7771 and λ7775 for both LTE and NLTE results. The absolute mean value of the correction is 0.12 dex with a maximum of 0.18 dex, less than the NLTE correction result of Schuler et al. (2006), in which O abundance derived from λ6300 is 0.28 dex lower than that derived from λ7774 for metal-rich cool giants. In our work, [O/Fe] shows 0.6-dex overabundance for [Fe/H] < -0.5, a decrease below [Fe/H] ~ 0.1, and they keep constant after [Fe/H] > 0.1.

The behaviour of O abundance with an NLTE correction for [Fe/H] < 0.1 is generally consistent with those of Soubiran & Girard (2005) (see Fig. 9) which give a large catalogue from the literature of disc stars. It is also consistent with most work on giants and disc stars for [Fe/H] < 0 (see e.g. King 1994, 2000 and references therein for giants, and e.g. Nissen et al. 2002; Bensby et al. 2004 for disc stars). However, there are discrepancies for supersolar metallcities ([Fe/H] > 0.1). For example, Nissen et al. (2002) found that [O/Fe] ~ 0 while Bensby et al. (2004) found that [O/Fe] continue to decrease after [Fe/H] > 0. Therefore, we can consider that the behaviour of oxygen abundance after the NLTE correction in cool giants has no obvious difference with that in disc stars, except for few stars with

Table 8. Abundances of six elements for the 63 nearby red clump giants relative to Fe.

Star	[Ca/Fe]	[Si/Fe]	[Ti/Fe]	[Ni/Fe]	[V/Fe]	[Ba/Fe]
HD 360	−0.03	0.09	0.00	0.03	−0.08	0.17
HD 770	−0.12	0.11	−0.06	0.02	−0.06	−0.04
HD 3750	−0.18	0.16	−0.16	0.10	−0.03	−0.19
HD 4188	0.01	0.17	−0.03	0.00	0.07	0.06
HD 4211	0.03	0.09	0.25	0.07	0.33	−0.01
HD 5268	0.12	0.20	0.04	0.00	−0.12	0.06
HD 5722	0.03	0.13	−0.01	0.02	−0.07	0.23
HD 6559	0.08	0.04	0.16	0.11	0.12	0.05
HD 6976	−0.03	0.05	0.09	0.01	0.01	0.17
HD 8651	0.06	0.16	0.13	0.03	0.03	0.02
HD 9362	0.06	0.17	0.00	0.06	−0.09	0.03
HD 10042	0.11	0.28	0.17	0.10	0.08	−0.06
HD 10142	−0.04	0.12	0.02	0.06	−0.06	−0.09
HD 10537	0.07	0.07	−0.01	0.00	0.07	0.04
HD 11643	−0.06	0.11	−0.06	0.07	0.08	−0.12
HD 15471	−0.07	0.18	0.05	0.10	0.04	−0.06
HD 15779	0.04	0.12	0.04	−0.01	0.02	0.10
HD 16815	0.15	0.12	0.19	0.01	−0.03	0.04
HD 16975	0.09	0.07	0.03	0.03	−0.08	0.32
HD 17652	0.10	0.17	0.10	0.02	0.00	0.03
HD 17824	0.06	0.04	0.01	−0.05	−0.04	0.31
HD 24706	−0.06	0.10	−0.03	0.12	0.26	−0.08
HD 25170	0.03	0.09	0.02	0.00	0.05	−0.10
HD 26967	0.10	0.06	0.01	0.01	0.11	−0.03
HD 120452	0.02	0.14	0.01	0.01	0.02	0.05
HD 138289	0.03	0.13	−0.05	−0.05	0.03	0.14
HD 139254	−0.06	0.20	0.08	0.09	0.20	−0.18
HD 140573	−0.17	0.22	0.00	0.09	0.04	−0.32
HD 141680	−0.01	0.14	0.00	0.03	−0.07	0.02
HD 142198	0.00	0.15	−0.02	−0.01	−0.08	0.08
HD 143546	0.09	0.15	0.02	0.00	−0.03	0.48
HD 143787	−0.06	0.14	−0.03	0.01	0.16	−0.07
HD 144046	0.05	0.11	−0.06	−0.05	−0.05	0.14
HD 146388	−0.12	0.17	−0.13	0.02	0.02	0.01
HD 146791	0.00	0.09	−0.06	−0.02	−0.08	0.23
HD 146686	−0.04	0.08	0.06	0.10	−0.02	−0.02
HD 147700	0.01	0.18	−0.03	0.02	−0.09	0.24
HD 149324	0.00	0.13	0.14	0.03	0.11	−0.07
HD 159433	0.04	0.08	0.07	0.02	0.07	0.01
HD 160315	−0.13	0.07	−0.09	−0.01	−0.16	−0.01
HD 166464	−0.02	0.14	−0.07	0.02	−0.02	0.22
HD 167768	0.18	0.31	0.08	−0.08	−0.01	0.10
HD 169916	0.01	0.05	−0.02	−0.02	0.05	0.07
HD 169767	0.05	0.15	0.11	0.03	0.04	0.11
HD 176704	−0.12	0.12	0.05	0.21	0.22	−0.23
HD 177241	−0.01	0.11	−0.01	−0.03	−0.03	0.14
HD 177873	−0.01	0.11	0.06	−0.02	0.11	0.13
HD 189561	−0.04	0.11	−0.07	−0.01	−0.10	0.20
HD 188887	−0.13	0.16	−0.08	0.01	0.09	−0.14
HD 191584	−0.13	0.25	−0.03	0.14	0.20	−0.17
HD 196171	0.00	0.13	−0.07	0.00	0.00	0.08
HD 204381	0.06	0.02	0.02	−0.03	−0.04	0.28
HD 214122	−0.04	0.09	−0.02	0.03	0.11	0.11
HD 215104	−0.03	0.14	−0.04	−0.04	−0.06	0.13
HD 216763	0.02	0.12	−0.02	−0.06	−0.07	0.26
HD 219449	0.06	0.14	0.02	0.04	−0.01	0.00
HD 219615	0.23	0.25	0.19	0.04	0.00	0.05
HD 219784	−0.07	0.15	−0.04	0.09	0.03	−0.01
HD 220572	−0.06	0.12	−0.04	0.04	−0.02	0.12
HD 220954	−0.08	0.10	−0.07	−0.02	0.06	−0.14
HD 221115	0.07	0.02	0.04	−0.06	−0.12	0.19
HD 222493	0.01	0.09	0.10	0.06	−0.02	−0.07
HD 223252	0.04	0.06	−0.01	−0.05	−0.12	0.14

Table 9. O abundance derived from triplet LTE results and after correction according to Takeda (2003).

Star	EW_{7772} (mÅ)	EW_{7774} (mÅ)	EW_{7775} (mÅ)	LTE				Δ_{NLTE}			
				$[O/Fe]_{7772}$	$[O/Fe]_{7774}$	$[O/Fe]_{7775}$	$[O/Fe]_{\overline{LTE}}$	$[O/Fe]_{7772}$	$[O/Fe]_{7774}$	$[O/Fe]_{7775}$	$[O/Fe]_{\overline{NLTE}}$
HD 360	40.3	38.7	24.6	0.14	0.23	0.01	0.08	−0.13	−0.13	−0.10	−0.04
HD 770	43.8	44.2	32.7	0.36	0.50	0.40	0.38	−0.14	−0.14	−0.11	0.26
HD 3750	32.9	40.4	36.9	0.12	0.47	0.59	0.36	−0.11	−0.11	−0.11	0.25
HD 4188	43.1	41.6	33.8	0.17	0.26	0.27	0.22	−0.14	−0.14	−0.12	0.09
HD 4211	42.6	–	35.4	0.31	–	0.46	0.39	−0.13	−0.05	−0.11	0.27
HD 5268	48.8	44.1	32.4	0.50	0.54	0.46	0.48	−0.15	−0.14	−0.11	0.35
HD 5722	46.4	44.4	32.8	0.26	0.35	0.27	0.27	−0.15	−0.15	−0.11	0.14
HD 6559	45.0	43.3	32.1	0.25	0.34	0.24	0.25	−0.14	−0.14	−0.11	0.12
HD 6976	39.3	35.9	27.3	−0.02	0.02	−0.03	−0.03	−0.13	−0.12	−0.10	−0.14
HD 8651	46.0	43.3	34.1	0.44	0.51	0.48	0.46	−0.15	−0.14	−0.12	0.33
HD 9362	41.2	38.8	27.3	0.33	0.40	0.28	0.31	−0.13	−0.13	−0.10	0.19
HD 10042	53.1	53.0	38.6	0.54	0.67	0.56	0.55	−0.17	−0.17	−0.13	0.40
HD 10142	43.6	43.5	36.0	0.34	0.47	0.48	0.41	−0.14	−0.14	−0.12	0.28
HD 10537	36.2	33.0	25.4	0.26	0.30	0.27	0.27	−0.12	−0.12	−0.10	0.16
HD 11643	32.3	43.8	31.6	0.04	0.50	0.37	0.21	−0.11	−0.11	−0.10	0.10
HD 15471	40.9	47.7	33.5	0.24	0.55	0.37	0.31	−0.13	−0.12	−0.10	0.19
HD 15779	41.7	41.8	32.5	0.12	0.26	0.21	0.17	−0.13	−0.14	−0.11	0.05
HD 16815	37.6	34.0	23.3	0.31	0.35	0.23	0.27	−0.12	−0.12	−0.09	0.17
HD 16975	54.2	55.3	42.5	0.07	0.23	0.15	0.11	−0.17	−0.18	−0.14	−0.05
HD 17652	38.3	35.9	26.8	0.27	0.34	0.29	0.28	−0.13	−0.12	−0.10	0.17
HD 17824	51.3	47.7	39.1	0.12	0.17	0.18	0.15	−0.16	−0.16	−0.13	0.01
HD 24706	28.7	38.1	27.0	0.14	0.57	0.42	0.28	−0.10	−0.10	−0.09	0.19
HD 25170	32.0	34.3	26.0	0.11	0.32	0.26	0.19	−0.11	−0.09	−0.09	0.09
HD 26967	31.7	32.6	23.4	0.07	0.23	0.12	0.10	−0.11	−0.09	−0.08	0.00
HD 120452	47.4	44.3	36.4	0.27	0.33	0.33	0.30	−0.15	−0.14	−0.12	0.17
HD 138289	38.4	35.5	28.4	0.19	0.26	0.25	0.22	−0.13	−0.12	−0.10	0.11
HD 139254	34.5	43.3	32.6	0.20	0.58	0.48	0.34	−0.11	−0.11	−0.10	0.24
HD 140573	32.8	57.2	39.2	0.06	0.76	0.52	0.29	−0.11	−0.14	−0.12	0.18
HD 141680	46.1	42.7	31.9	0.39	0.45	0.37	0.38	−0.15	−0.14	−0.11	0.25
HD 142198	42.3	40.1	30.4	0.35	0.43	0.37	0.36	−0.14	−0.13	−0.11	0.24
HD 143546	62.6	64.1	45.8	0.33	0.49	0.31	0.32	−0.20	−0.22	−0.15	0.15
HD 143787	25.7	27.9	21.9	0.15	0.36	0.34	0.25	−0.10	−0.10	−0.09	0.15
HD 144046	53.8	55.0	39.1	0.17	0.33	0.17	0.17	−0.18	−0.14	−0.12	0.02
HD 146388	37.3	46.1	30.6	0.09	0.46	0.23	0.16	−0.12	−0.15	−0.11	0.05
HD 146791	47.6	44.0	30.5	0.17	0.22	0.08	0.13	−0.15	−0.14	−0.11	−0.01
HD 146686	45.1	47.5	36.5	0.12	0.31	0.23	0.18	−0.14	−0.15	−0.12	0.05
HD 147700	51.6	44.9	34.6	0.46	0.44	0.38	0.42	−0.16	−0.15	−0.12	0.28
HD 149324	36.2	43.7	30.1	0.11	0.45	0.27	0.19	−0.12	−0.14	−0.11	0.08
HD 159433	31.2	32.8	23.8	0.34	0.53	0.44	0.39	−0.11	−0.09	−0.08	0.30
HD 160315	46.6	49.1	36.4	0.05	0.24	0.13	0.09	−0.15	−0.16	−0.12	−0.05
HD 166464	41.6	42.3	31.9	0.15	0.31	0.22	0.19	−0.13	−0.14	−0.11	0.07
HD 167768	57.0	54.9	41.1	0.81	0.90	0.82	0.82	−0.18	−0.18	−0.13	0.66
HD 169916	29.3	30.4	23.3	−0.09	0.08	0.05	−0.02	−0.11	−0.11	−0.09	−0.12
HD 169767	34.8	32.3	30.6	0.19	0.26	0.41	0.30	−0.12	−0.11	−0.11	0.19
HD 176704	34.7	52.1	36.6	0.06	0.65	0.45	0.26	−0.11	−0.11	−0.11	0.15
HD 177241	46.4	39.0	27.4	0.23	0.17	0.04	0.14	−0.15	−0.13	−0.10	0.01
HD 177873	36.4	38.8	26.4	0.13	0.34	0.16	0.15	−0.12	−0.13	−0.10	0.04
HD 189561	60.8	58.6	42.3	0.41	0.50	0.34	0.38	−0.19	−0.19	−0.14	0.21
HD 188887	33.6	33.0	25.0	0.27	0.38	0.31	0.29	−0.11	−0.09	−0.08	0.20
HD 191584	44.4	58.3	34.6	0.55	0.95	0.61	0.58	−0.14	−0.15	−0.11	0.46
HD 196171	41.2	43.0	34.7	0.14	0.32	0.32	0.23	−0.13	−0.14	−0.12	0.11
HD 204381	55.8	52.4	40.8	0.10	0.16	0.10	0.10	−0.18	−0.17	−0.13	−0.06
HD 214122	35.5	32.4	26.8	0.15	0.18	0.21	0.18	−0.12	−0.11	−0.10	0.07
HD 215104	45.8	42.0	35.8	0.37	0.42	0.47	0.42	−0.15	−0.14	−0.12	0.29
HD 216763	47.5	43.4	31.6	0.31	0.35	0.25	0.28	−0.15	−0.14	−0.11	0.15
HD 219449	39.6	42.2	27.6	0.26	0.46	0.23	0.25	−0.13	−0.14	−0.10	0.13
HD 219615	53.7	48.6	36.7	0.73	0.75	0.69	0.71	−0.17	−0.16	−0.12	0.57
HD 219784	36.6	44.3	34.2	0.28	0.62	0.55	0.42	−0.11	−0.11	−0.11	0.31
HD 220572	43.9	44.7	33.1	0.18	0.33	0.22	0.20	−0.14	−0.15	−0.11	0.08
HD 220954	40.6	42.0	32.3	0.10	0.29	0.21	0.16	−0.13	−0.14	−0.11	0.04
HD 221115	54.6	51.6	37.6	0.10	0.17	0.05	0.08	−0.17	−0.17	−0.13	−0.08
HD 222493	56.6	58.5	47.2	0.17	0.35	0.31	0.24	−0.18	−0.19	−0.15	0.08
HD 223252	49.4	51.1	37.7	0.08	0.25	0.15	0.16	−0.16	−0.17	−0.13	−0.03

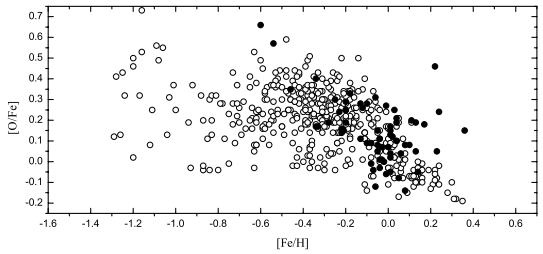

Figure 9. The NLTE abundance of O with those of Soubiran & Girard (2005).

[Fe/H] > 0.1 which show overabundance. This overabundance may be due to the fact that NLTE corrections for metal-rich stars (0.09–0.14 dex) are underestimated comparing with that in Schuler et al. (2006). In our case, however, only a few stars with [Fe/H] > 0.1 were studied; to obtain a more conclusive result, we might need to exploit NLTE approximation based on a larger sample.

Cunha & Smith (2006) found that in old low-mass Galactic bulge red giants, the ^{16}O abundances have not been altered measurably due to red giant dredge-up. Schuler et al. (2006) had calculated the evolution model of the Hyades giants for $M = 2.5\,M_{\odot}$ and found that there is no obvious alternation of ^{16}O during the first dredge-up, and this negligible change in O abundance is also reproduced in Sweigart, Greggio & Renzini (1989), Charbonnel (1994) and Boothroyd & Sackmann (1999). Our data show that the O abundance has no obvious difference with that of disc stars; therefore, we believe that the ^{16}O abundance has not been changed after the stars experienced the first dredge-up of their red giant stage. According to theoretical prediction by Iben (1991), ^{16}O is partially converted into ^{14}N in the central regions of the main-sequence stars. However, the convective envelope hardly reaches the O-depleted region during the first dredge-up for the mass range considered here (see e.g. fig. 1 of Charbonnel 1994). As a consequence, surface O variations are very well consistent with theory.

6.3 α-elements

Like O, Mg is mainly produced from SNe II. In our work, the Mg abundance ratio varies in a way similar to that of [O/Fe]. First, it shows a tendency to decrease with increasing metallicity for $-0.6 <$ [Fe/H] < 0.1, and it keeps almost constant for $0.1 <$ [Fe/H] < 0.4. The flattening trend towards high metallicity of Mg is also traced in Edvardsson93 and Chen00 (see Fig. 10). If, as nucleosynthesis theory predicts, O and Mg are mainly produced from SNe II, and Fe is mainly generated by SNe Ia, the flat trend of [Mg/Fe] towards high metallicity is unexpected. It seems that SNe II are not the only contributor to Mg production, and SNe Ia may be another source for Mg.

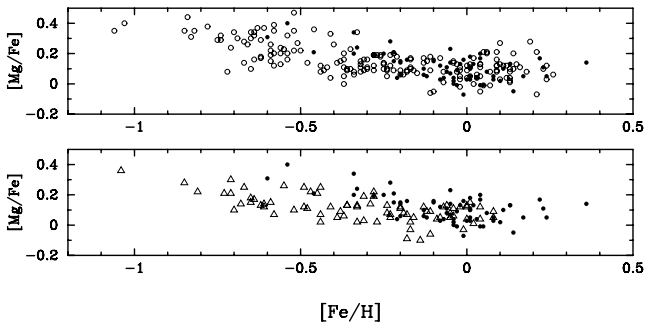

Figure 10. The mean abundance of Mg elements. Upper panel: our result compared with that of Edvardsson et al. (1993). Lower panel: our result and that of. The filled circles, open triangles and open circles represent data of our work, Chen et al. (2000) and Edvardsson et al. (1993), respectively.

Silicon is a prototypical α-element, and is expected to be synthesized mainly in moderate-mass ($\sim 20\,M_{\odot}$) SNe II (Woosley & Weaver 1995). [Si/Fe] exhibits an enhancement in metal-poor stars, as found in most studies of metal-poor stars. However, it keeps unchanged for $-0.3 <$ [Fe/H] < 0.1, and has a little upturn for [Fe/H] > 0.1. The abundance trend for our [Si/Fe] is similar to that of Edvardsson93, even the upturn trend is seen in their work, whereas it is absent in Chen00. However, the mean value of [Si/Fe] is a bit higher than those of Edvardsson93 and Chen00. It seems that the offset is due to systematic errors.

Calcium is produced in the same process as used for the production of silicon, and it is found to be enhanced in metal-poor stars (McWilliam et al. 1995). The abundance pattern for [Ca/Fe] in our results is basically matched with that of Edvardsson93. However, the flat trend for [Fe/H] > 0.0 found in McWilliam et al. (1995) and Chen00 is not obvious in our work, where it keeps on declining while the metallicity is increasing.

As Ti exhibits an enhancement in metal-poor stars, it is traditionally referred to as an α-elements. [Ti/Fe] slightly decreases with increasing metallicity, and this trend becomes less obvious towards higher metallicity, which supports the results of Edvardsson93 and Chen00. Both Si and Ca have a very small star-to-star scatter; however, Ti and Mg have a relatively large star-to-star scatter.

The mean [α/Fe] (Mg, Si, Ca and Ti) is shown to be a decreasing function of [Fe/H], smoother than that of Edvardsson93 and Chen00 (see Fig. 11).

Zhao et al. (2001c) analysed 39 red clump giants and gave the abundance of [α'/H] defined in Edvardsson93, which is the mean

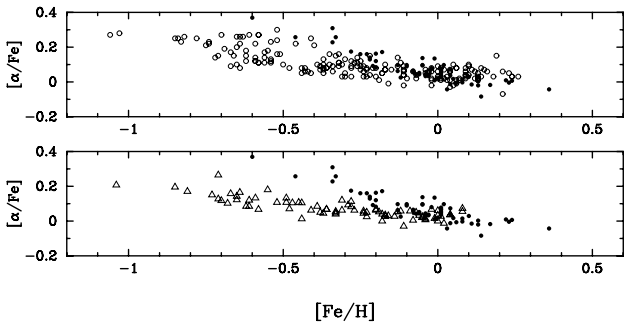

Figure 11. The mean abundance of α-elements. Upper panel: our result compared with that of Edvardsson93. Lower panel: our result and that of . The filled circles, open triangles and open circles represent data of our work, Chen et al. (2000) and Edvardsson et al. (1993), respectively.

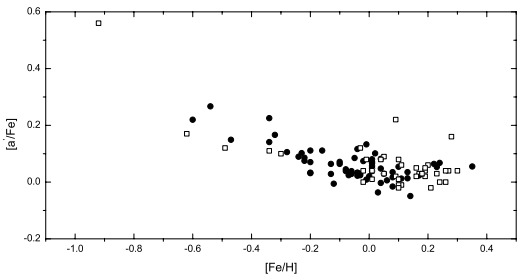

Figure 12. Comparison of [α'/Fe] of our result with that of Zhao et al. (2001c). The filled circles and open squares represent data of our work and Zhao et al. (2001c), respectively.

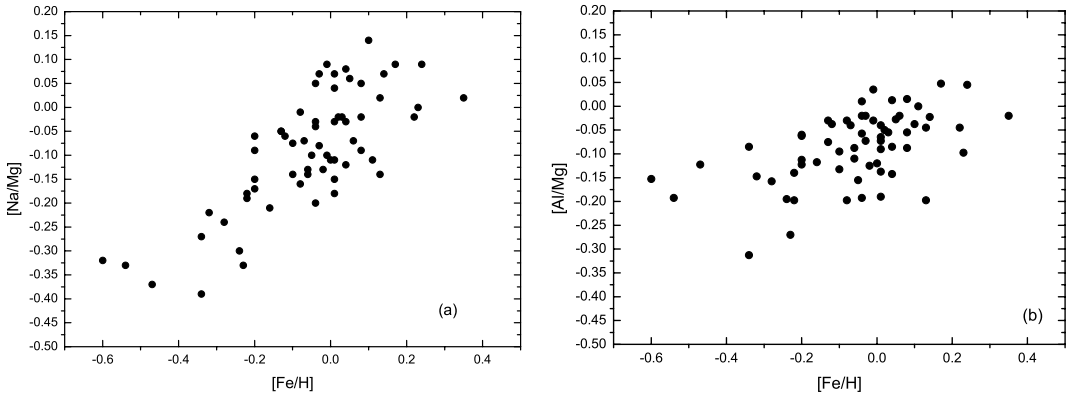

Figure 13. NLTE result on element ratios for [Na/Mg](a) and [Al/Mg](b) as a function of metallicity.

value of [Si/H] and [Ca/H]. Being the same type of stars, a comparison between [α'/Fe] of our work and that of Zhao et al. (2001c) is very important. We present the result of our data together with that of Zhao et al. (2001c) in Fig. 12 showing that the two data samples are well consistent.

6.4 Sodium and aluminum

Na and Al are thought to be produced in SNe II and SNe Ib/c, with probably only a small contribution of SNe Ia (Nomoto, Thielemann & Yokoi 1984). A part of the available neutron flux depends on the initial metallicity and therefore initial oxygen abundance, which is in turn crucial to nucleosynthesis. Therefore, in stars with only slightly subsolar abundances, one expects a rapid increase in [Na, Al/Mg] ratios in proportion to the iron abundance. In Fig. 13, we find this smooth increase in [Na/Mg] as a function of metallicity, but a relatively mild increase in [Al/Mg].

According to stellar evolution theory, the surface abundance of Na will be enriched as a result of the Na–Ne cycle operation during the first dredge-up phase, and has also been found overabundance in many studies of giants and supergiants (e.g. Andrievsky et al. 2002; Mishenina et al. 2006). In our work, the NLTE abundance of Na scales well with Fe for [Fe/H] < 0, and a mild upturn when [Fe/H] $>$ 0.0 with a mean value of 0.1 dex. This upturn is reproduced in disc stars (Edvardsson93; Feltzing & Gustafsson 1998; Shi et al. 2004). However, Mishenina et al. (2006) found Na overabundance of about 0.1 dex for the whole metallicity coverage from -0.7 to 0.3. This diversity may be due to the fact that adopted lines and atomic data are different. The NLTE trend of Na in our sample seems to be not different from that in dwarfs (see Fig. 14), which is not expected according to stellar evolution theory.

There is an indication of higher [Al/Fe] at lower metallicity (Tomkin, Lambert & Balachandran 1985, Edvardsson93). As such, Al is sometimes classified as an α-element. However, Chen00 found a different trend in Al abundance, with [Al/Fe] ~ 0 at lower metallicity [Fe/H], which is suggested to be due to NLTE effect. Our results with an NLTE correction show that the abundances of Al are consistent with those of Edvardsson93, see Fig. 15.

6.5 Iron-peak elements

Spectral lines with hyperfine structure (HFS) appear broader than those without HFS. Vanadium is a well-known example for HFS. In solar-type stars, the effect of HFS for weak lines can be neglected. However, it is crucial to take this effect into account in our stars,

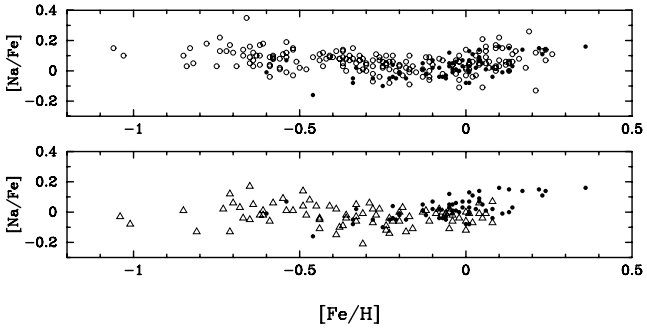

Figure 14. The NLTE abundance of Na with those of Edvardsson93 and Chen00.

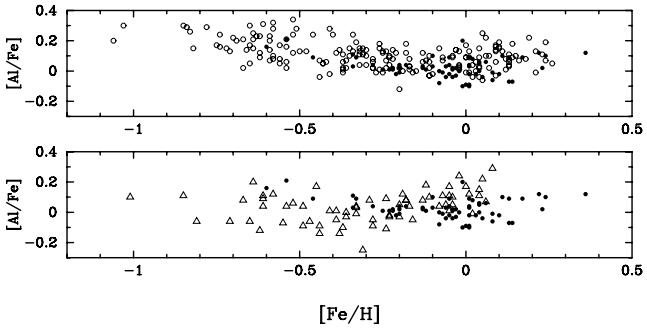

Figure 15. The NLTE abundance of Al with those of Edvardsson93 and Chen00.

since the vanadium lines are strong and are broadened by strong line splitting. We can see from Fig. 16 that the abundance corrections due to the introduction of HFS are between 0.01 and 0.5 dex. The HFS data we have adopted are taken from Kurucz.[4]

Vanadium keeps in step with Fe (e.g. Chen00), and in our work vanadium seems to follow Fe for the whole metallicity range, with a little higher value in metal-rich stars. This trend basically supports the nucleosynthesis theory, which suggests that the Fe group is mainly produced from SNe Ia, and all its members should keep in step with the iron abundance. The overabundance of V in metal-rich stars is also found in Feltzing & Gustafsson (1998), who explained it as a result of overionization and/or hyperfine splitting, and Schuler et al. (2004, 2006) also found that overexcitation/ionization

[4] http://Kurucz.harvard.edu/linelists.html.

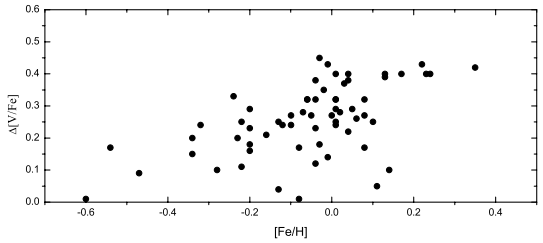

Figure 16. The difference in vanadium abundances obtained neglecting HFS minus those including HFS versus metallicity. Δ[V/Fe] on *Y*-axis represents $\log V_{\text{non-HFS}} - \log V_{\text{HFS}}$.

may work in cool dwarfs. However, it does not seem to work in giants (Schuler et al. 2006). In our calculations, the HFS effect is considered, and no overionization was shown (see Fig. 4), so the overabundance may be due to the HFS effect more than we estimated in metal-rich stars or it really exists in metal-rich stars.

The abundance of Ni varies in lockstep with metallicity with a possible upturn for [Fe/H] > 0.1. This upturn is also evident in the data of Edvardsson93. Whether it is real needs to be testified by more metal-rich samples. For the same metallicity coverage, the Ni trend in our work is the same as that in Chen00.

6.6 Barium

Due to the lack of good-quality absorption lines, we analyse Ba as the only element heavier than the iron group in our work. As is seen in Edvardsson93, our result indicates that Ba keeps flat for $-0.6 <$ [Fe/H] < 0, and then decreases towards higher metallicities. The abundance trend of Ba for [Fe/H] > 0.0 is similar to that in Chen00, who found that [Ba/Fe] increased with metallicity for [Fe/H] < -0.7, and then keeps a constant small overabundance in the range of $-0.7 <$ [Fe/H] < -0.2 and decreases again for [Fe/H] > -0.2. Mashonkina & Gehren (2000) found that Ba is slightly underabundant by 0.1 dex relative to iron in the thick disc stars. However, Chen00 found [Ba/Fe] overabundance of about 0.1 dex in the range $-0.8 <$ [Fe/H] < -0.2. Mashonkina et al. (2000) explained this discrepancy by an NLTE effect that leads to a 0.2-dex overestimate of [Ba/Fe] on average when using λ5853, λ6141 and λ6496. As we also used these three lines, the NLTE effects are significant, and they cause an overestimate of [Ba/Fe] of at least 0.2 dex in the metallicity range $-0.6 <$ [Fe/H] < -0.2 for our sample.

Ba is thought to be a product of the s-process in low-mass asymptotic giant branch (AGB) stars, which have a longer evolutionary time-scale than that of iron contributor SNe Ia. [Ba/Fe] decreasing with metallicity ([Fe/H] > 0.0) is not consistent with the nucleosynthesis theory. The possible reason which Chen00 suggested could be that an s-element synthesis occurs less frequently in metal-rich AGB stars possibly because the high mass loss finishes their evolution earlier.

7 CONCLUSIONS

We analyse the abundances of 10 elements for 63 nearby red clump giants with iron abundances ranging from -0.6 to 0.36 dex. Our main results and conclusions are summarized below.

(1) The Mg, Si, as well as V, Ni and Ba in red clump giants follow the same trends as found in solar type disc stars (e.g. Edvardsson93, Chen00).

(2) The abundance trends of Ti and Ca are slightly different from those of Edvardsson93. Ti and Ca continue to decrease slowly towards higher metallicities rather than keeping unchanged as in Edvardsson93. However, the decreasing trend is so marginal that we can consider that Ti and Ca keep the same trend as that of solar-type stars.

(3) The surface abundance of O in red clump giants is not changed after they experienced the first dredge-up, which is consistent with the prediction of the Galactic evolution theory.

(4) The abundances of Na, Mg and Al are determined by an NLTE approximation and the NLTE effects for Na, Mg and Al are from -0.10 to -0.24, -0.05 to 0.02 and -0.05 to -0.14, respectively.

(5) In the case of the metal-rich stars, the abundance results for Na and Al are fairly confusing. Chen00 found both [Na/Fe] and [Al/Fe] ~ 0.0 for the whole metallicity range of the disc stars. However, Edvardsson93 found that Na and Al are overabundant in some metal-rich stars, and that Al is enhanced in metal-poor stars. The abundances of Na and Al in our work are in agreement with those of Edvardsson93. However, the abundance of Na may alter during the first dredge-up; however, this enrichment is not seen in our sample.

(6) Although V is well known to be broadened by HFS, this was neglected in most of the work on disc stars, since the lines are not very strong and HFS effects would cause errors less than 0.1 dex. However, in red clump giants, the HFS effect cannot be ignored, and it will cause 0.01–0.5 dex abundance differences in our sample stars.

ACKNOWLEDGMENTS

We are thankful to Prof. Thomas Gehren for valuable comments and many stimulating discussions. This work was funded by the National Natural Science Foundation of China under grant number 10521001, 10433010 and 10403006. GP and WG gratefully acknowledge financial support received from the Chilean Centre for Astrophysics FONDAP 15010003. We would like to thank the referee 's valuable and comments and suggestions.

REFERENCES

Alonso S., Arribas S., Martínez-Roger C., 1999, A&AS, 140, 261
Alonso S., Arribas S., Martínez-Roger C., 2001, A&A, 376, 1039
Andrievsky S. M., Egorova I. A., Korotin S. A., Burnage R., 2002, A&A, 389, 519
Bard A., Kock M., 1994, A&A, 282, 1014
Bard A., Kock A., Kock M., 1991, A&A, 248, 315
Bensby T., Feltzing S., Lundström, 2004, A&A, 415, 155
Blackwell D. E., Menon S. L. R., Petford A. D., Shallis M. J., 1982a, MNRAS, 201, 611
Blackwell S. L. R., Petford A. D., Shallis M. J., Simmons G. J., 1982b, MNRAS, 199, 43
Boothroyd A. I., Sackmann I. J., 1999, ApJ, 565, 587
Butler K., Mendoza C., Zeippen C. J., 1993, J. Phys. B, 26, 4409
Carpenter J. M., 2001, AJ, 121, 2851
Cayrel de Strobel G., Soubiran C., Friel E. D., Ralite N., Francois P., 1997, A&AS, 124, 299
Charbonnel C., 1994, A&A, 282, 811
Chen Y. Q., Nissen P. E., Zhao G., Zhang H. W., Benoni T., 2000, A&AS, 141, 491 (Chen00)
Cunha K., Smith V. V., 2006, ApJ, 651, 491
Cutri R. M. et al., 2003, Explanatory Supplement to the 2MASS All Sky Data Release, http://www.ipac.caltech.edu/2mass/releases/allsky/doc/explsup.html
Drawin H. W., 1968, Z. Phys., 211, 404
Drawin H. W., 1969, Z. Phys., 225, 483
Edvardsson B., Andersen J., Gustafsson B., Lambert D. L., Nissen P. E., Tomkin J., 1993, A&A, 275, 101 (Edvardsson93)

Eriksson K., Toft S. C., 1979, A&A, 71, 178
ESA, 1997, The Hipparcos and Tycho Catalogues, ESA SP-1200
Feltzing S., Gustafsson B., 1998, A&AS, 129, 237
Gehren T., Butler K., Mashonkina L., Reetz J., Shi J., 2001, A&A, 366, 981
Gehren T., Liang Y. C., Shi J. R., Zhang H. W., Zhao G., 2004, A&A, 413, 1045
Gehren T., Shi J. R., Zhang H. W., Zhao G., Korn A. J., 2006, A&A, 451, 1065
Geisler D., Clariá J., Minniti D., 1991, AJ, 102, 1836
Girardi L., Bressan A., Bertelli G., Chiosi C., 2000, A&AS, 141, 371
Grevesse N., 1984, Phys. Scripta, T8, 49
Gratton R. G., Carretta E., Eriksson K., Gustafsson B., 1999, A&A, 350, 955
Hauck B., Mermilliod M., 1998, A&AS, 129, 431
Iben I. Jr., 1991, ApJS, 76, 55
King J. R., 1994, AJ, 107, 350
King J. R., 2000, ApJ, 120, 1056
Kiselman D., 1991, A&A, 245, 9
Kiselman D., 1993, A&A, 275, 269
Kubiak M., McWilliam A., Udalski A., Górski K., 2002, AcA, 52, 159
Kurucz R. L., 1993, CD-ROM No.13,18 Smithsonian Astrophysical Observatory
Mashonkina L., Gehren T., 2000, A&A, 364, 249
Mashonkina L., Gehren T., Travaglio C., Borkova T., 2003, A&A, 397, 275
McWilliam A., 1990, ApJS, 74, 1075 (McW90)
McWilliam A., 1997, ARA&A, 35, 503
McWilliam A., Preston G. W., Sneden C., Searle L., 1995, AJ, 109, 2757
Mishenina T. V. et al., 2006, A&A, 456, 1109
Nissen P. E., Edvardsson B., Gustafsson B., 1985, in Danziger I. J., Mateucci F., Kjär K., eds, Proc. ESO Workshop, Production and Distribution of C,N,O Elements. ESO, Garching, p. 131
Nissen P. E., Primas F., Asplund M., Lambert D. L., 2002, A&A, 390, 235
Nomoto K., Thielemann F.-K., Yokoi K., 1984, ApJ, 286, 644
O'Brian T. R., Wickliffe M. E., Lawler J. E., Whaling J. W., Brault W., 1991, J. Opt. Soc. Am. B, 8, 1185
Paczyński B., Udalski A., Szymański M., Kubiak M., Peitrzyński G., Soszyński I., Woźniak P., Żebruń K., 1999, AcA, 49, 319
Persson S. E., Murphy D. C., Krzeminski W., Roth M., Rieke M. J., 1998, AJ, 116, 2475
Schuler S. C., Jeremy R. K., Hobbs L. M., Pinsonneault M. H., 2004, ApJ, 602, L117
Schuler S. C., Hatzes A. P., King J. R., Kürster M., The L. S., 2006, AJ, 131, 1057
Skrutskie M. F. et al., 2006, AJ, 131, 1163
Shi J. R., Gehren T., Zhao G., 2004, A&A, 423, 683
Soubiran C., Girard P., 2005, A&A, 438, 139
Sweigart A. V., Greggio L., Renzini A., 1989, ApJS, 69, 911
Takeda Y., 2003, A&A, 402, 343
Takeda Y., Kawanomoto S., Sadakane K., 1998, PASJ, 50, 97
Taylor B. J., 1999, A&AS, 134, 523
Tautvaišienė G., 1997, MNRAS, 286, 948
Tinsley B. M., Larson R. B., 1979, MNRAS, 186, 503
Tomkin J., Lambert D. L., Balachandran S., 1985, ApJ, 290, 289
VandenBerg D. A., 1992, ApJ, 391, 685
Woosley S. E., Weaver T. A., 1995, ApJS, 101, 181
Yi S. K., Kim Y. C., Demarque P., 2003, ApJS, 144, 259
Zhao G., Gehren T., 2000, A&A, 362, 1077
Zhao G., Qiu H. M., Zhang H. W., 2001a, ChA&A, 25, 59
Zhao G., Li H. B., 2001b, ChJA&A, 6, 555
Zhao G., Qiu H. M., Mao S., 2001c, ApJ, 551, 85

SUPPLEMENTARY MATERIAL

The following supplementary material is available for this article online:

Table 1. All atomic-line data used and EW values of programme stars.

This material is available as part of the online article from: http://www.blackwell-synergy.com/doi/abs/10.1111/j.1365-2966.2007.11852.x. (This link will take you to the article abstract.)

Please note: Blackwell Publishing are not responsible for the content or functionality of any supplementary materials supplied by the authors. Any queries (other than missing material) should be directed to the corresponding author for the article.

This paper has been typeset from a TEX/LATEX file prepared by the author.